INSTABILITY, TRANSITION AND RECEPTIVITY OF PULSATILE FLOW IN A STENOTIC TUBE

H M BLACKBURN[1] and S J SHERWIN[2]

[1] CSIRO Manufacturing and Materials Technology, PO Box 56, Highett, Victoria 3190, AUSTRALIA

[2] Dept Aeronautics, Imperial College London, South Kensington Campus, London SW7 2AZ, UK

ABSTRACT

This work examines pulsatile flow in a straight tube with an axisymmetric constriction that reduces the local cross-sectional area by 75%. The model is a much-simplified representation of physiological flow in an artery that has a constriction produced by atherosclerotic plaque. Through linear stability analysis of the axisymmetric flow we find that there are two different global absolute modes leading to localised turbulent transition. Both of these are associated with vortex rings that are blown out of the contraction during each pulse. Using DNS we show that the turbulent bursts move upstream to lie close to the stenosis, even though the instability modes have maximum energy far downstream. Under suitable conditions, the vortex rings may trail extended shear layers in their wakes, and these are receptive to noise through a convective instability mechanism. The shear layer instability can also interact with, and promote, the vortex-ring instabilities.

NOMENCLATURE

D tube diameter
k azimuthal wavenumber
L stenosis length
p pressure
r radial coordinate
Re Reynolds number
t time
t_0 phase point in pulse period
T pulse period
$\boldsymbol{u}$ velocity
u_m area-average velocity
U_{red} reduced velocity
z axial coordinate

α Womersley number
ε perturbation
μ Floquet multiplier
σ Floquet exponent
θ azimuthal coordinate
ν kinematic viscosity

INTRODUCTION

Stenotic geometries typically occur in initially healthy arteries as a result of atherosclerotic lesions that form in the wall of the vessel. It is known that there is a close connection between arterial disease and local flow features that lead to low and fluctuating wall shear stresses (e.g. flow separation). Also, it is not uncommon to find multiple inline stenoses in diseased individuals. These findings have stimulated a number of CFD studies of flows in stenotic geometries, from highly idealised representations through to detailed reconstructions derived from individual patients. Our work addresses the fundamentals of instability mechanisms with an idealised axisymmetric geometry and a simple, single-harmonic, non-reversing pulsatile inflow, in order to form a basis for understanding more complex real flows.

Geometry and inflow

The geometry of the stenosis is shown in **Figure 1**(a). The origin of our (z, r, θ) coordinate system is at the centre of the throat. The particular geometry chosen has $D/D_{min}=2$ (on the basis that this is the minimum constriction in diameter that can reliably be detected using ultrasound), also $L/D=2$, and is a sinusoidal shape.
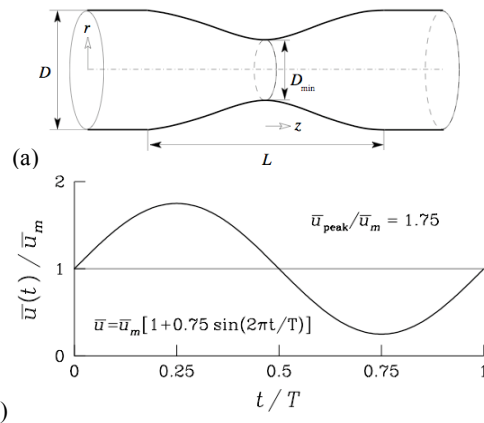
Figure 1: Schematic diagram of stenosis geometry, and of the area-averaged inflow condition.

The area-averaged inflow waveform is the sum of a steady mean flow u_m a single harmonic of relative amplitude 0.75 and period T, so that the ratio of peak:mean flow is 1.75, as illustrated in **Figure 1**(b). While the mean flow can be represented by the Hagen-Poiseuille parabolic profile, the profiles of oscillatory components must be represented using (complex) Bessel functions, as originally shown by Sexl (1930). These can be added together linearly, since the nonlinear terms in the Navier-Stokes equations reduce to zero for parallel incompressible flows. Two dimensionless groups that describe the remainder of the problem are the Reynolds number $Re=u_m D/\nu$, and a reduced velocity $U_{red}=u_m T/D$. The reduced velocity can be considered as a dimensionless pulse period. An alternative non-independent dimensionless number often used in this area of work is the Womersley parameter $\alpha=(\pi Re/2 \; U_{red})^{1/2}$. We have used the reduced velocity so that the effects of viscosity are represented only in the Reynolds number.
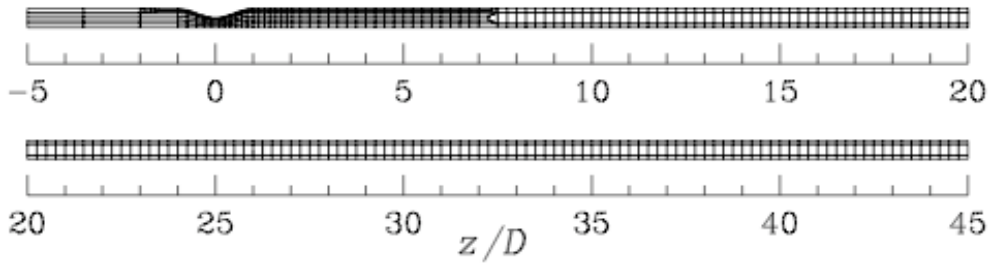
Figure 2: Spectral element mesh for discretisation of the meridional semiplane in cylindrical coordinates.
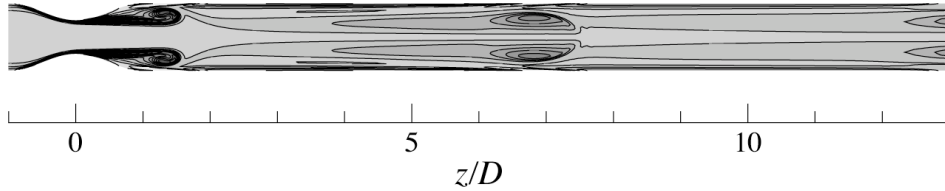
Figure 3: Example of an axisymmetric flow, for Re=400 and U_{red}=2, at one instant of the pulse cycle. Contours of vorticity.

METHOD

Our investigation couples numerical Floquet analysis of the stability of axisymmetric pulsatile flows to three-dimensional disturbances and three-dimensional direct numerical simulation (DNS) of the growth of instabilities to turbulence. The stability analysis, which is based on time integration of the linearised Navier-Stokes equations (see e.g. Tuckerman & Barkley 2000), uses the same underlying discretisation as the DNS.

The incompressible Navier-Stokes equations are treated in cylindrical coordinates using a mixed implicit-explicit pseudospectral velocity correction scheme that is second-order in time. Spatial discretisation is carried out using Gauss-Lobatto-Legendre nodal basis spectral elements in the meridional semiplane and Fourier expansions in the azimuthal direction. Details of the discretisation are supplied in Blackburn and Sherwin (2004), where exponential spatial convergence of the method is demonstrated for non-axisymmetric flows.

The spectral element macro mesh used is shown in Figure 2. There are 743 spectral elements, concentrated around the stenosis throat and where the shear layers are thinnest. A spectral element basis function order N_p=7 was found to be adequate for both stability analysis and for DNS computations. A comparatively long outflow length was found necessary in order to capture the Floquet instability modes, which can reach their greatest amplitude far downstream of the stenosis.

Temporal Floquet analysis examines the behaviour of a perturbation u' to a T-periodic base flow U, to determine whether the perturbation grows or decays from cycle to cycle. In a linear analysis, the evolution equations for the perturbation flow are the Navier-Stokes equations linearised about the base flow. Perturbation solutions can be written as a sum of Floquet modes $u(t_0)\exp[\sigma(t-t_0)]$ where $u(t_0)$ is a T-periodic Floquet eigenfunction, evaluated at arbitrary phase t_0 and σ is a Floquet exponent. Floquet multipliers μ are related to the Floquet exponents by μ=exp(σT), and indicate how much the Floquet modes grow (or shrink) from cycle to cycle. In general, the exponents, the multipliers, and the eigenfunctions can be real or occur in complex-conjugate pairs. Instability occurs when a multiplier leaves the unit circle, μ=1, or equivalently when the real part of a Floquet exponent becomes positive. In the present treatment, Floquet modes can take any spatial form supported in a fixed frame of reference by the global (r, z) discretisation and hence by definition an unstable Floquet mode is a global (absolute) instability.

Stability analysis is computed using a hybrid block-power-Krylov method described by Tuckerman and Barkley (2000), and Blackburn (2002). The method relies on the repeated application of an operator (here, the linearised Navier-Stokes equations, integrated over a period T) rather than explicit computation of the equivalent matrix operator, and delivers a small number of leading modes.

AXISYMMETRIC BASE FLOWS

An example of an axisymmetric flow, visualised through contours of vorticity, is shown in Figure 3. It should be noted that approximately 1/3rd of the computational domain is represented in this figure. Just downstream of the stenosis throat (near z/D=1), a vortex ring that is in the process of rolling up can be seen in section. Further along the tube (near z/D=7) is the vortex ring from the previous pulse cycle, and at z/D=13, the vortex ring from the pulse cycle previous again is seen as it leaves the visualised region. Another significant feature of the vorticity field are the shear layers that trail in the wake of each vortex ring.

A comparison of the axial locations of vortex rings at the same phase point t_0, but at various reduced velocities, is shown in Figure 4. Immediately evident is the fact that the initial dimensionless speed of the vortex rings is approximately 3, independent of pulse period. The asymptotic dimensionless speed of the rings tends towards a value of unity (which is the mean speed of the time-average flow), although the process is only able to complete at the higher reduced velocities. This can be attributed to the fact that the vorticity in the rings diffuses away more quickly at smaller pulse periods, and individual rings become difficult to identify comparatively rapidly.
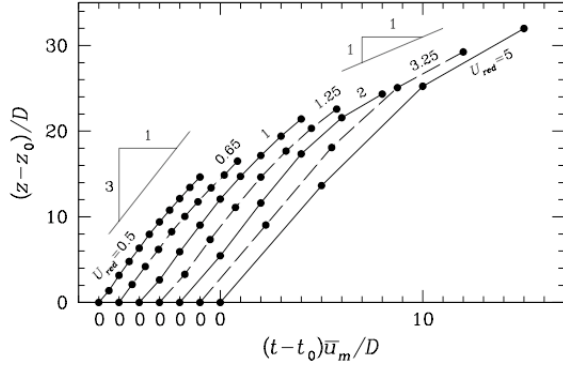
Figure 4: Dimensionless axial locations of base flow vortex rings as a function of dimensionless time (ring formation index times U_{red}) at various values of U_{red}, all computed at Re=400.

The relative uniformity of the initial speeds is remarkable given that the amount of vorticity which is shed from the detachment point near the stenosis throat per pulse must increase with pulse period, and that the propagation velocity of vortex rings is approximately linearly related to the amount of circulation they contain. The resolution of this apparent paradox is that the vortex rings at the head of each pulse must contain approximately the same amount of initial circulation, independent of pulse period, while the `excess' shed vorticity is left in the shear layers that trial in the wakes of the rings. These shear layers become more extensive at higher reduced velocities. Similar behaviour has been noted for the production and propagation of individual vortex rings into unconstrained fluid by Rosenfeld, Rambod and Gharib (1998).

A further feature that can be observed in Figure 4 is that at the same Reynolds number, vortex rings survive longer as identifiable features when the reduced velocity is increased.

THREE-DIMENSIONAL GLOBAL INSTABILITIES

We have found two kinds of global instabilities for these flows. At high values of reduced velocity, the dominant mode is a period-doubling instability that is associated with alternating tilting of the vortex rings blown out of the throat on successive pulses (Sherwin and Blackburn 2005). The mode has azimuthal wavenumber k=1, and becomes unstable as the associated Floquet multiplier leaves the unit circle along the negative real axis, i.e. μ_c=−1.. The alternation is caused by a coupled wake downwash effect: as one vortex ring in a pair tilts in one direction, its asymmetric wake flow drives the succeeding vortex ring to tilt in the opposite direction. At lower values of reduced velocity, wavy vortex-core instabilities become dominant (Blackburn and Sherwin 2006). A pair of modes, with azimuthal wavenumber k=3 and k=4 respectively, compete for dominance over a narrow range of reduced velocity. These are synchronous modes, i.e. μ_c=+1. The marginal stability curves in (U_{red}, Re) control space for the two kinds of modes are shown in Figure 5. In both cases, there is an `optimal' reduced velocity for which the critical Reynolds number is lowest: for the period-doubling mode, this occurs near U_{red}=3.25, while of the wavy modes it occurs near U_{red}=0.875.
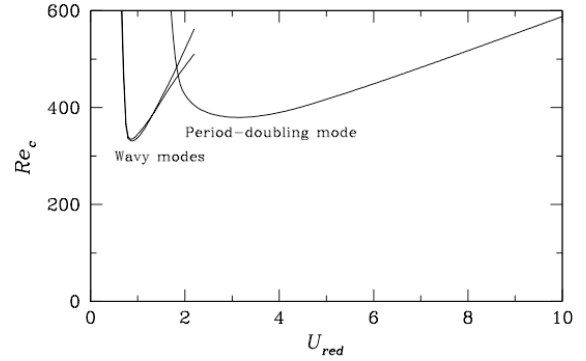
Figure 5: Marginal stability curves for the two kinds of global three-dimensional instabilities.

Floquet modes

The association between energy in the base flows and in the instability modes near the optimal reduced velocities is illustrated in Figure 6. In the panel (a) we see the instantaneous energy in the base flow at U_{red}=3.25, Re=370, while in (b) we see the logarithm of energy in the period-doubling Floquet mode. Regions of concentrated kinetic energy in the base flow correspond to the locations of vortex rings. The regions of concentrated energy in the Floquet mode are seen also to correspond to the locations of base flow vortex rings, which means that the rings supply the energy that drives the instability mode. In panels (c) and (d) we see corresponding results for the k=3 wavy mode at U_{red}=0.875, Re=325. Again there is a clear association between the energy in the Floquet mode and vortex rings of the base flow.

Note that the axial location of peak Floquet mode energies is typically many diameters downstream of the stenosis, and that Floquet mode energy initially increases in the downstream direction even though energy in the base flows dies away monotonically. However, since the Floquet modes are ultimately dependent on energy in the base flows for growth, they also eventually reduce in energy along a streamwise traverse.

At the 'optimal' reduced velocities for the two types of modes, the location of the kinetic energy of the Floquet modes reaches its most upstream location; for reduced velocities either higher or lower than these optima the Floquet mode energy moves further from the stenosis. Since the axial spacing of successive vortex rings increases with U_{red}, the ring-to-ring overlap of energy in the Floquet modes (evident in Figure 6, b and d) reduces, and there is less cooperative interaction between the instabilities that grow on successive vortex rings. On the other hand, the vortex rings survive longer as reduced velocities increase (see Figure 4). It appears that a competition between these two effects gives rise to the existence of an `optimal' reduced velocity for each type of global Floquet mode.

Nonlinear evolution

Nonlinear evolution of the global instabilities is examined using DNS. The axisymmetric base flow is projected from two to three spatial dimensions, and is seeded with a small amount of the global instability mode, to form a three-dimensional initial condition, which is integrated forward in time.
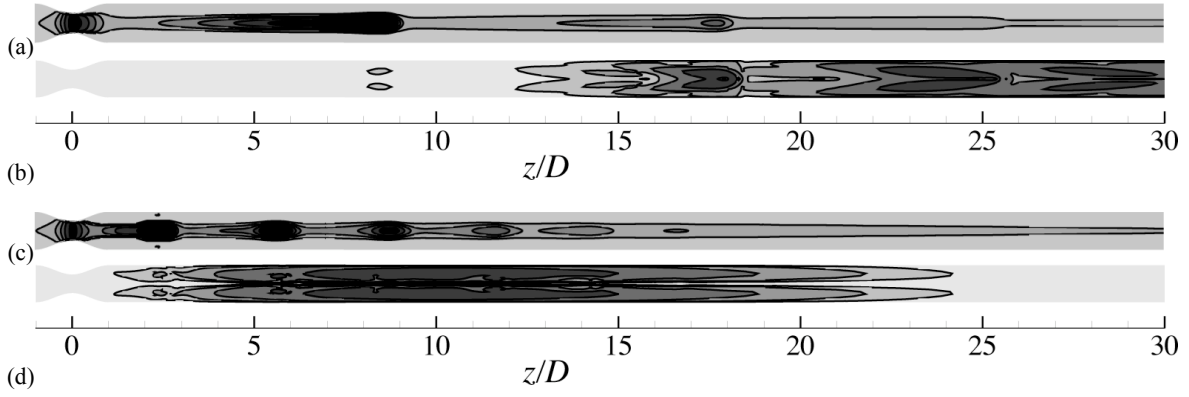
Figure 6: Contours of instantaneous kinetic energy of base flows and logarithm of the energy in the corresponding Floquet mode. (a, b): U_{red}=3.25, Re=370; (c, d): U_{red}=0.875, Re=325.
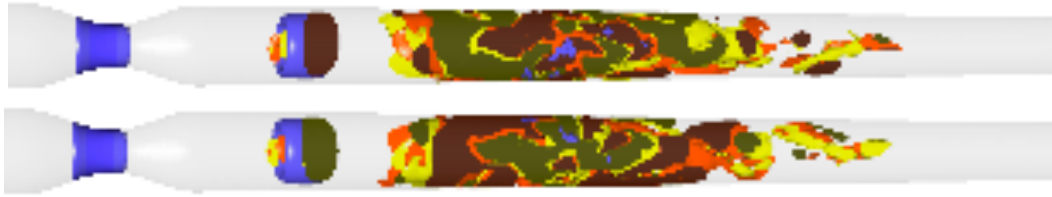
Figure 8: Illustration of the vortex-tilting instability after it has progressed to turbulent transition. The two images show the flow one pulse period apart; note the almost exact reflection symmetry, which is a consequence of the period-doubling nature of this mode. Blue: positive value of velocity gradient discriminant, red/yellow: positive/negative values of axial vorticity. U_{red}=2.5, Re=400.

Figure 9: Illustration of the k=3 wavy instability after it has progressed to turbulent transition. Isosurfaces as for figure 8. U_{red}=1, Re=350.

The resulting flows can take many hundreds of pulse cycles to reach asymptotic turbulent states. The typical evolution is first to an initial nonlinear saturation (which can be approximated using a simplified normal form model), and which will result in a weakly turbulent burst located near that of maximum Floquet mode energy. This is followed by a much slower nonlinear growth phase, in which the flow three-dimensional energy grows, and the axial location of the turbulent bursts moves upstream. An example of a state achieved after the initial nonlinear saturation, for a k=3 wavy mode, is seen in Figure 7.
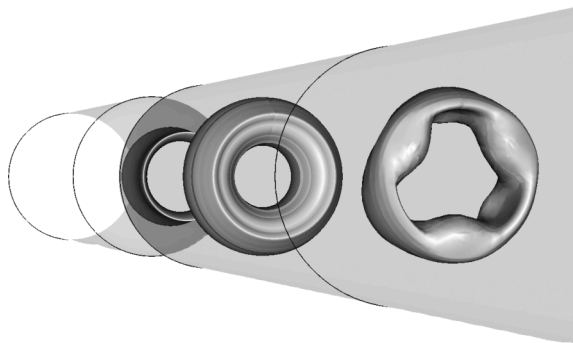
Figure 7: Visualisation of the k=3 wavy instability, after it reaches an initial nonlinear saturation. The wavy vortex ring closest to the viewpoint undergoes a breakdown almost immediately. U_{red} = 1, Re=350.

Examples of the states achieved at the end of the slower nonlinear growth phase are shown in Figures 8 and 9. Figure 8 represents the final stage of evolution for the vortex-tilting mode, shown at two times, one pulse period apart. Vortex rings are visualised using an isosurface (blue) drawn at a positive level of the discriminant of the velocity gradient tensor; inside such isosurfaces, the local nature of the flow is spiralling, either in or out (Blackburn, Mansour and Cantwell 1996). Three-dimensional distortion of the vortex rings is emphasised by drawing (red/yellow) isosurfaces of streamwise vorticity component (a quantity that is zero in an axisymmetric flow). By comparing the first vortex ring structure in the parallel part of the tube downstream of the stenosis in the upper and lower panels of Figure 8, one can observe the alternate ring-tilting nature of the instability. Further downstream the instability progresses to a breakdown event, and again, the approximate reflection symmetry of the upper and lower panels of Figure 8 is related to the period-doubling nature of the underlying linear instability. Further downstream again, the flow relaminarises. Note that the location of the turbulent breakdown (of order $5D$ downstream of the stenosis) is much closer to the stenosis than the location of the greatest Floquet mode energy, which, as seen in Figure 6(b), is of order $20D$ downstream of the stenosis. By this upstream movement, the instability is able to extract more energy from the base flow, since the vortex rings are most intense near where they form.

Figure 10: Roll-up of the separated shear layer of steady flow at *Re*=700, when perturbed by a small-amplitude, high-frequency (U_{red}=0.3) oscillation of the inflow. Isosurface of azimuthal vorticity.

Figure 9 shows a corresponding result for the asymptotic state of a wavy instability. The underlying three-fold symmetry of the underlying linear instability is still apparent in this image (especially around the first identifiable vortex ring downstream of the stenosis), although a high degree of distortion is also evident. Again, the location of the final turbulent breakdown is well upstream of the location of maximum Floquet mode energy (of order 10*D* downstream of the stenosis, see Figure 6d).

AXISYMMETRIC CONVECTIVE INSTABILITIES

As reduced velocity is increased, the vortex rings that lead each pulse structure trail extended shear layers, as explained above. And while steady flows in this geometry become three-dimensionally unstable at *Re*=722 (Blackburn and Sherwin 2005), they always exhibit an initially axisymmetric shear layer emanating from a separation in the stenosis throat. Both these types of extended shear layer are susceptive to a convective instability (i.e. one that will wash out of the domain if not perturbed). In order to examine this mechanism, we have driven the flow by adding an very small, high-frequency periodic excitation on the inflow, the amplitude of which, 0.001, is too small to be visually evident on the inflow.

Convective instability of steady flow

First we examine convective instability of steady flow for Reynolds numbers below the onset of the first global mode, which is a weak Coanda instability. Figure 11 illustrates the response of the flow to the perturbation by plotting the normalised energy in the perturbation flow as functions of reduced velocity of the perturbation, and of Reynolds number. Evidently the flow is most responsive to perturbation in a comparatively narrow band of reduced velocities centred around U_{red}=0.35, which leads to shear-layer rollups, as seen in Figure 10.
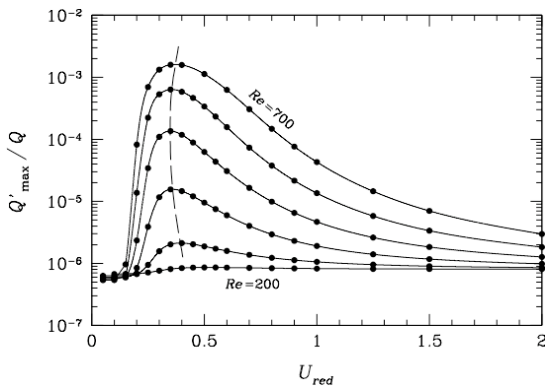
Figure 11: Convective instability results for axisymmetric steady flows. These show the domain integral of kinetic energy in the difference between the perturbed flow and the steady flow, normalised by the domain integral of energy in the corresponding steady flow, as functions of reduced velocity of the perturbation, and Reynolds number.

Convective instability of pulsatile flow

Now turning to pulsatile base flows, again we add a small high-frequency (low reduced velocity) perturbation to the inflow boundary condition of the axisymmetric flows and examine the response in terms of the relative energy in the perturbation flow. Sample outcomes for three different reduced velocities of base flows are shown in Figure 12. The pulsatile flows at lower reduced velocities (0.875 and 3.25, respectively the optima for the wavy and period-doubling instabilities) are comparatively unresponsive to perturbation, while the flow for U_{red}=10 is much more responsive, over a spectrum of perturbation reduced velocity centred around U_{red}=0.2, about one-half the most responsive value for steady flow. As for the steady flow case, the physical nature of the response is a convective-type shear layer oscillation, which is typically only active over the portion of the pulse cycle for which the shear layers are significant visual features of the flow.
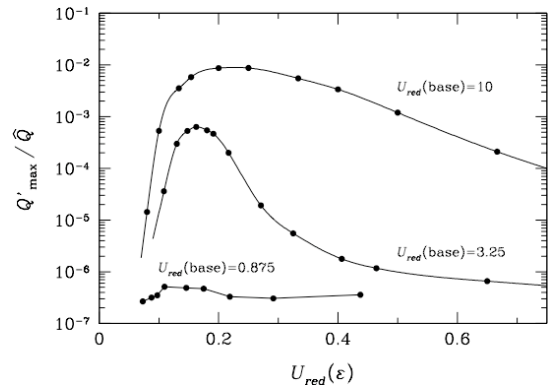
Figure 12: Convective instability results for axisymmetric pulsatile flows. Peak domain-integral energy in the perturbation flow normalised by peak energy in the unperturbed flow when a high-frequency, low-level harmonic forcing at reduced velocity $U_{\mathrm{red}}(\varepsilon)$ is added to the inlet of three pulsatile flows. Reynolds numbers for the three base flows at U_{red}=0.875, 3.25 and 10 were respectively 350, 400 and 600.

The fact that receptiveness of the pulsatile flows to perturbation grows with the reduced velocity of the perturbed flow is related directly to the phenomenon discussed above in relation to the base flows that the shear layers that trail in the wake of the vortex rings become more and more extended as reduced velocity increases. The comparatively weak and short-lived shear layers that may occur for smaller reduced velocities are not nearly as susceptible to convective instability.

Interaction of global and convective instabilities

It is possible for the convective instability of the pulsatile flow to interact with the global Floquet instability. In order to examine this, the base flow chosen for Floquet analysis is the periodic state achieved with a high-frequency component $U_{\mathrm{red}}(\varepsilon)$ chosen for peak response (as in figure 12) added to the regular pulsatile flow. The stability analysis is carried through by linearising about